ATLANTIS PRESS

Atlantis Highlights in Engineering (AHE), volume 2

International Conference on Industrial Enterprise and System Engineering (IcoIESE 2018)

On the Relationship of Travel Time and Energy Efficiency of Industrial Robots

Kai Eggers, Zygimantas Ziaukas, Jens Kotlarski, Tobias Ortmaier
Gottfried Wilhelm Leibniz Universität Hannover
Institute of Mechatronic Systems
Hanover, Germany
Email: firstname.lastname@imes.uni-hannover.de

***Abstract*—This paper presents an approach to quantify the energy saving potential with regard to travel time of industrial robot motions. In order to minimize the influence of the exemplary considered trajectories and, thus, provide general results, the evaluation is done on a large set of automatically generated point-to-point motions on a KUKA KR 210 serial robot. For this purpose, an energy model specifically tailored to industrial robots is introduced, along with an algorithm for automatic generation of appropriate evaluation trajectories. It is shown that the power consumption model requires an accurate inverse dynamics and friction model, while simplified models of motors and invertes yield sufficient results.**

***Index Terms*—Industrial Robotics, Energy Efficiency, Efficient Trajectory Planning, Travel Time**

I. Introduction

Sales of industrial robots reached an all time high of 248,000 units sold in 2015 worldwide, increasing by about 12 % compared to the previous year [1]. In the future, ongoing significant growth is expected. A rising degree of automation leads to an increase of overall energy consumption. At the same time, manufacturers aim to reduce production costs to stay competitive in the dynamic global market and sustainability becomes more and more a matter of interest regarding the companies' image and the requirement to meet legal regulations. Due to these developments, the reduction of energy consumption becomes evermore relevant.
In the past, several hardware-based energy efficiency approaches have been developed, e. g. the reduction of moved masses by lightweight design [2] or the development and application of high efficient drive components [3]. Further, recent research presented methods to reduce the energy consumption by optimizing the utilized path planning algorithms [4]–[11]. These software-based optimizations can be applied without any additional hardware cost and without (or with minor) production downtime, which makes them highly viable.

In order to optimize the path planning for a given application, the process needs to provide certain degrees of freedom by allowing a modification of the travel time and/or a change of the geometrical path. Mostly, this is possible for point-to-point (PTP) motions. Tasks with a predefined Cartesian trajectory, such as line welding or adhesive bonding, usually require a specific path velocity. Hence, they provide neither of the aforementioned requested degrees of freedom.

One possible optimization approach aims at finding the energy-optimal travel time for a given trajectory without altering the geometrical path [4], [5]. If the considered motion is not time-critical for the whole process, travel time can be exceeded without affecting the overall cycle time. A longer travel time causes a reduction of dynamic losses on the one side, but an increase of gravitational losses on the other side. Hence, it is assumed that an energy-optimal travel time can be found leading to minimal (cumulated) losses.

However, the above mentioned publications [4]–[11] focus on case studies with a small number of evaluation trajectories. In consequence, this paper aims to provide general information on the relationship of travel time and power consumption for industrial robots. To achieve this, a set of 1000 automatically generated PTP tasks is applied to a KUKA KR 210 industrial robot. For evaluation purposes, a model of the system's overall energy consumption that correctly depicts the energy consumption in different operating points (i. e. different velocities, torques, accelerations, and, consequently, different travel times) is introduced. The proposed modelling approach including validation measurements is presented in section II. The trajectory generation algorithm is explained in section III. Several simulation results are given and discussed in section IV. The paper closes with a conclusion in section V.

II. Model of System Energy

Comprehensive energy demand modelling approaches for mechatronic systems have been presented in existing publications, e. g. [12], [13]. However, the proposed model is specifically designed for industrial robots, which enables significant model complexity reductions while maintaining high accuracy. This leads to advantages in feasibility, computation time, and system identification effort. Assuming that the parameters of the inverse dynamics model are known, the presented power

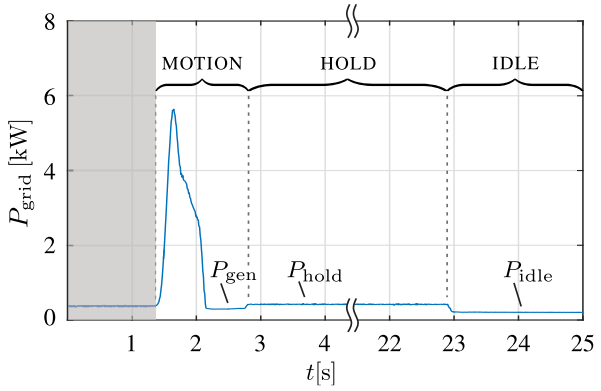

Fig. 1. Typical power consumption measurement for an industrial robot in different operating phases

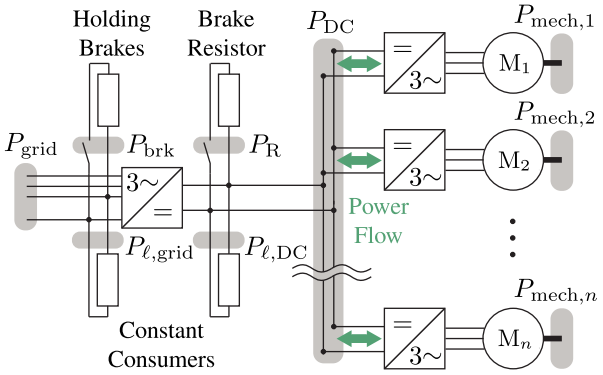

Fig. 2. Electrical substitute circuit diagram for an industrial robot

model uses only three additional parameters that can be identified in a single power measurement. The correct simulation and comparison of the energy consumption at different travel times requires a model representing the consumption while in motion as well as in standstill. In order to clarify different power consumption phases, a typical power measurement for a PTP motion is shown in Fig. 1. The operational state can be divided into three different phases:

- MOTION means that the robot is currently moving,
- HOLD describes a robot in active control with lifted holding brakes, while
- IDLE signifies that the holding brakes have been applied.

The causes of power consumption in the different phases are explained in section II-A, along with the identification of the required parameters. The modelling of the motion-dependent power consumption is formulated in section II-B. Validation measurements are presented in section II-C.

A. Operating Phases

The power consumption during the different operating phases can be explained by consideration of a simplified electrical substitute circuit diagram (Fig. 2). During the MOTION phase, the power consumption depends on the robot's mechanical power demand $P_{\mathrm{mech},i}$ that is induced by the given motion. A detailed description of the modelling approach on this particular term can be found in section II-B. The sum of mechanical powers is represented by an auxiliary variable P_{DC} that characterizes the power flow within the DC bus. Since most state-of-the-art robot controls are not able to recuperate, excess power P_{R} is dissipated through a brake resistor. All further DC bus losses are summarized as a constant loss power $P_{\ell,\mathrm{DC}}$. Constant losses on the grid side are split into two groups: the power P_{brk} is required to keep the brakes lifted while $P_{\ell,\mathrm{grid}}$ summarizes the constant losses of all peripheral components (e. g. controller, cooling fans, IO modules, sensors, etc.).

During the IDLE phase, all the components on a 600 V level are inactive and the holding brakes are applied. Hence, the measurable power P_{idle} equals $P_{\ell,\mathrm{grid}}$. In the HOLD phase, the power demand is induced by the constant losses on the grid side, on the DC side, and by the brake lifting power:

$$P_{\mathrm{hold}} = P_{\ell,\mathrm{grid}} + P_{\ell,\mathrm{DC}} + P_{\mathrm{brk}}. \tag{1}$$

The power consumption at static holding is not considered separately. It is instead included in the constant DC losses $P_{\ell,\mathrm{DC}}$. The dependency on the robot configuration is neglected: measurements have shown a maximum deviation of P_{hold} of approx. 5 % for the KUKA KR 210 in the most extreme poses (see section II-C for test bed description). However, with regard to the robot's peak power of approx. 20 kW (see Fig. 4), deviation is less than 0.01 %.

Industrial robots usually feature backlash free gears with high friction. Hence, the mechanical losses clearly exceed the electrical ones and the proposed simplifications only have a minor impact on the grid power consumption (see also section II-C). The main advantage of this approach is the significant reduction of required parameters which enables the model for application on an industrial level.

B. Motion-dependent Power Consumption

This section focuses on the calculation of the motion-dependent power consumption. Assuming that a trajectory of an industrial robot is predefined, the calculation of the system power demand starts with determining the motor torques $\tau(t)$. In general, the model of inverse dynamics is given by

$$\tau(t) = \mathrm{diag}\left(\frac{1}{u_{\mathrm{G},1}},\ldots,\frac{1}{u_{\mathrm{G},n}}\right)\left(M(q)\ddot{q} + c(q,\dot{q}) + g(q)\right) + h(q,\dot{q}), \tag{2}$$

where $q, \dot{q}, \ddot{q}$ are time-dependent joint angles, velocities, and accelerations given by the trajectory planning algorithm. The term $u_{\mathrm{G},i}$ represents the gear factor of joint i while the vector τ contains the respective motor torques τ_i. M contains moments of inertia, c Coriolis effects, and g gravitational effects. h summarizes non-linear effects which in our regarded case is merely friction. In [14], a commonly used friction model including Coulomb friction and viscous damping (coefficients $f_{\mathrm{c},i}$ and $f_{\mathrm{v},i}$, respectively) is presented. It is applied to this model, expressing friction torque $\tau_{\mathrm{f},i}$ of joint i as

$$\tau_{\mathrm{f},i}(t) = h_i(t) = f_{\mathrm{c},i}\ \mathrm{sign}(\omega_i(t)) + f_{\mathrm{v},i}\ \omega_i(t), \tag{3}$$

where ω_i is the angular motor velocity of motor i which can be determined as

$$\omega_i(t) = u_{\mathrm{G},i}\,\dot{q}_i(t). \tag{4}$$

Most robotic manufacturers utilize a model of the inverse dynamics within the robot control system for implementation of feed forward control. Thus, it can be assumed that the system friction parameters are known. If not, they can be obtained using established identification methods [15], [16]. Equations 2 and 4 are used to obtain the mechanical power $P_{\mathrm{mech},i}(t)$ of each motor i:

$$P_{\mathrm{mech},i}(t) = \tau_i(t)\ \omega_i(t). \tag{5}$$

The The total DC bus power P_{DC} is obtained by summing up the mechanical power of the n individual motors:

$$P_{\mathrm{DC}}(t) = \sum_{i=1}^{n} P_{\mathrm{mech},i}(t). \tag{6}$$

For state-of-the-art industrial robots, the DC bus features a capacitor that is usually dimensioned to smoothen the rectified voltage, not to buffer excess energy in generator operation phases. Hence, the capacity is neglected. However, it can be implemented according to [7] if desired. Further, the rectifiers in industrial robot cabinets are usually not able to recuperate. Hence, negative values of P_{DC} need to be partly corrected. The excess power in generator operating phases can cover the constant losses within the DC bus, but the grid side losses will remain. The remaining power consumption is marked as P_{gen} in Fig. 1. This behaviour is considered as follows:

$$\begin{aligned}
&P_{\mathrm{DC}}(t) + P_{\ell,\mathrm{DC}} \geq 0: \\
&\qquad P_{\mathrm{grid}}(t) = P_{\mathrm{DC}}(t) + P_{\ell,\mathrm{DC}} + P_{\ell,\mathrm{grid}} + P_{\mathrm{brk}}, \\
&\qquad P_{\mathrm{R}}(t) = 0, \\
&P_{\mathrm{DC}}(t) + P_{\ell,\mathrm{DC}} < 0: \\
&\qquad P_{\mathrm{grid}}(t) = P_{\mathrm{gen}} = P_{\ell,\mathrm{grid}} + P_{\mathrm{brk}}, \\
&\qquad P_{\mathrm{R}}(t) = -(P_{\mathrm{DC}}(t) + P_{\ell,\mathrm{DC}}),
\end{aligned}$$

where $P_{\mathrm{R}}(t)$ is the power dissipated via the brake resistor. The time integral of the grid power demand over trajectory time (from t_{start} to t_{end})

$$E_{\mathrm{grid}} = \int_{t_{\mathrm{start}}}^{t_{\mathrm{end}}} P_{\mathrm{grid}}(t)\ \mathrm{d}t \tag{7}$$

equals the grid energy demand of the system of a given trajectory.

C. Validation

The model is applied to and parameterized for a KUKA KR 210 with a maximum payload of 210 kg (actual permitted payload might be lower depending on the location of tool's center of mass). The robot is chosen because of the high market share of serial robots and a payload that is commonly used in automotive production. The test setup is shown in Fig. 3. The grid power is measured using a Yokogawa WT 3000 precision power analyzer. The robot is equipped with a test weight of 200 kg, shaped as specified by the manufacturer.

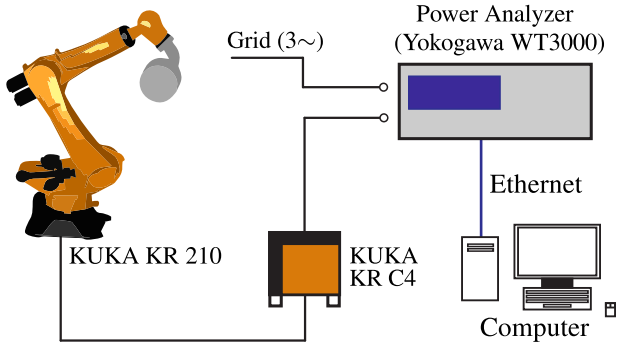

Fig. 3. Test bed setting for validation trajectory measurement

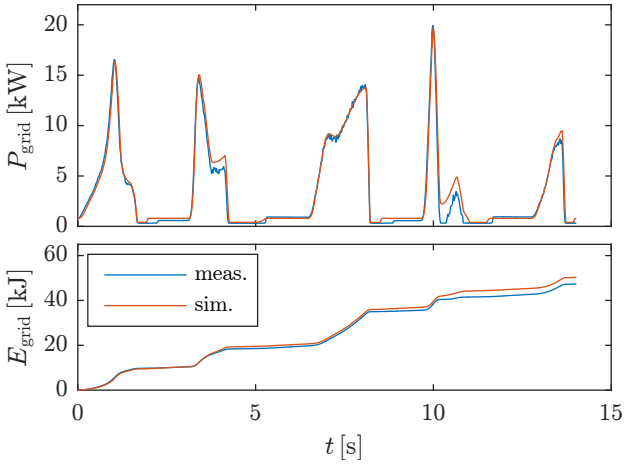

Fig. 4. Measured and simulated power demand at OR 100

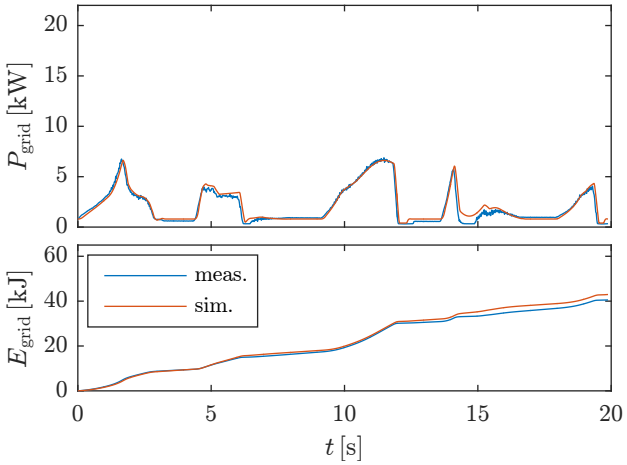

Fig. 5. Measured and simulated power demand at OR 60

The measured as well as the simulated power demand of the robot is shown in Fig. 4. The validation trajectory consists of five PTP motions, separated by one-second pauses. The resulting grid energy demand is slightly overestimated by the simulation by +5.3 %. The measurement is performed again with a different travel time. The travel time can be directly altered by utilizing the Override (OR) function that most robot controls provide. The OR affects the travel time T as follows:

$$T = T_{\min} \frac{100}{\mathrm{OR}}, \tag{8}$$

where $T_{\min}$ represents the minimal travel time achieved at maximum speed (OR 100). The measurement results are shown in Fig. 5. The deviation is comparable with an overestimation of +4.9 % by the simulation. Further measurements with varying trajectories and travel times delivered comparable results with an error within approx. ± 5 %. The validation results show that the model with the proposed complexity reductions, in contrast to existing complex models in current research, adequately depicts the real system's grid power and energy demand.

While different simplifications have been introduced for the modelling of the electrical part of the drive system, it is important to reach a high accuracy for the mechanical power model. Although there is a significant dependency between robot temperature and its power demand, previous works often neglect this. While [4], [17] consider the robot temperature, only the temperature dependencies of motor resistors are taken into account.

Figure 6 demonstrates the impact of robot (i. e. motor) temperature on its mechanical power demand. The values are based on the traced values at a KR 210 using its internal sensors. While the motor temperature ϑ_i does not equal the gear temperature, it sufficiently displays the robot's thermal state. The measured grid energy demand of the same motion at different temperatures is shown in Fig. 7. An enhanced modelling approach with temperature-dependent friction parameters will be presented in future works. In this paper, friction parameters were identified for motor temperatures of 60 °C. Unless stated otherwise, all presented measurements and results refer to this operating point.

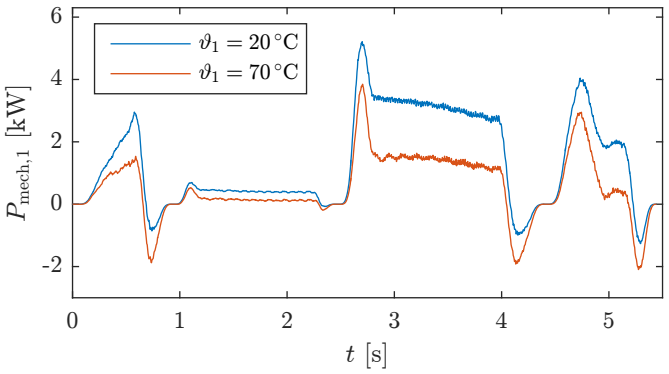

Fig. 6. Mechanical power comparison of axis $i = 1$ at different motor temperatures based on measured (traced) values for τ_1 and ω_1

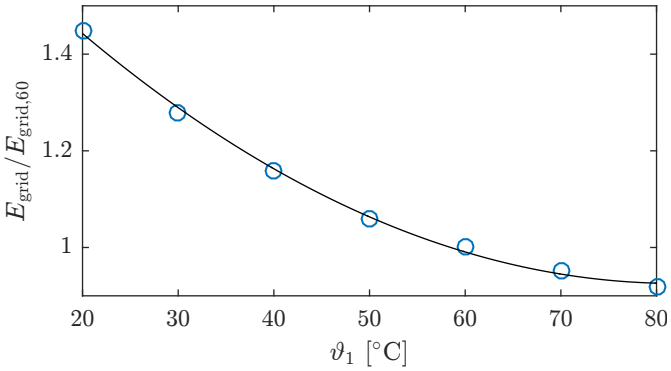

Fig. 7. Dependency of grid energy demand E_{grid} on temperature normalized to the grid energy demand $E_{\mathrm{grid},60}$ at 60 °C motor temperature

III. Generation of Evaluation Trajectories

This chapter presents the algorithm to automatically generate an arbitrary number of different plausible PTP tasks. The aim is to generate a set of trajectories that fulfills the following criteria:

- The entire accessible workspace should be utilized,
- the trajectories should feature motions for a varying number of involved joints,
- motions shorter than an adjustable threshold should be excluded from the evaluation.

For clarification, it is necessary to distinguish between trajectory (or motion) and task. While the trajectory provides the time-dependent set values for position, velocity, and acceleration, the task is defined by just the start and end configuration. Hence, the presented algorithm automatically generates PTP tasks, but the trajectory planning is done by the embedded robot motion controller. Due to this partition, it is ensured that the examinations feature state-of-the-art trajectory planning algorithms which are essential for providing meaningful results.

The tasks are generated as follows. First, based on the minimum and maximum joint angles, a vector with n_{eq} equidistant positions is generated. For example, for $n_{\mathrm{eq}} = 5$ positions and minimum and maximum angles of $q_{i,\min} = -20°$ and $q_{i,\max} = 100°$, possible positions of joint i are $(-20°, 10°, 40°, 70°, 100°)^{\mathrm{T}}$.

These values represent possible start and/or end positions of the considered joint. The tasks can be generated by randomly picking two of the generated configurations. It is allowed for each joint that the start position equals the end position (at least one joint has to move). An additional threshold $\Delta q_{\min}$ guarantees that at least one joint executes a motion of a predefined minimal distance. As stated above, the corresponding trajectories are generated using the robot motion

controller (in this case a KUKA KR C4). This leads to a set of trajectories that fulfills the aforementioned criteria. Note that self-collisions are innately avoided by design and joint angle boundaries of the regarded robots. Positions with a height lower than zero are considered as valid to take account for robots mounted on a pedestal.

IV. Evaluation

The model presented in section II is used to evaluate a set of 1000 PTP tasks, generated according to section III. The aim is to provide general and reliable results for the relation between travel time and power consumption of industrial robots. The evaluation procedure is first explained in detail for a single PTP task in section IV-A. Afterwards, the results for the whole set of trajectories are presented in section IV-B.

A. Single Task Evaluation

First, we examine the energy consumption of a single PTP task while gradually reducing the OR. The scaling is done by interpolating the given joint space trajectories with a new time vector so that the geometrical path remains unchanged. In order to correctly compare the energy consumption at different travel times, it is necessary to equalize the integration time within a set of geometrically identical PTP motions (identical tasks). The faster motions are augmented by HOLD and IDLE phases as described in section II-A, depending on the standstill duration in the HOLD phase and the brake application time t_{brk}.

The results for the first PTP task are shown in Fig. 8a. The graphic depicts the overall energy consumption E_{grid} for the same task at varying ORs (from OR 20 to OR 100) with a step size of five. As stated before, the OR is inversely porportional to the travel time, e. g. OR 20 induces a multiplication of travel time by five.

Due to the high default value for t_{brk} of 20 s, the IDLE phase is never reached in the considered scenarios. It can be observed that the energy consumption for the motion decreases with increasing travel time up to a certain point (in this case around OR 50) and then increases again. However, after adjusting the measuring periods by taking the waiting phases into account, the slowest motion is the most efficient one in this case.

The evaluation of the same scenario but with a theoretically ideal brake application time of $t_{\mathrm{brk}} = 0\,\mathrm{s}$ is shown in Fig. 8b. The standstill losses can be reduced and the energetic optimum shifts to approx. OR 50. It is important to note that a reduction of t_{brk} might shorten the machine's life span and should be carefully evaluated for the given process beforehand [18].

B. A Set Of 1000 PTP Tasks

The evaluation from the previous section is performed for a set of tasks that is generated according to section III with $n_{\mathrm{eq}} = 5$ and $\Delta q_{\mathrm{min}} = 50^{\circ}$. The grid energy consumption is normalized to the consumption at OR 100. Hence, the relative savings can be compared across different tasks. The simulation results for a KR 210 with the default $t_{\mathrm{brk}} = 20\,\mathrm{s}$ are visualized as a box plot in Fig. 9a. The red line indicates the median energy consumption at each OR while the blue box contains

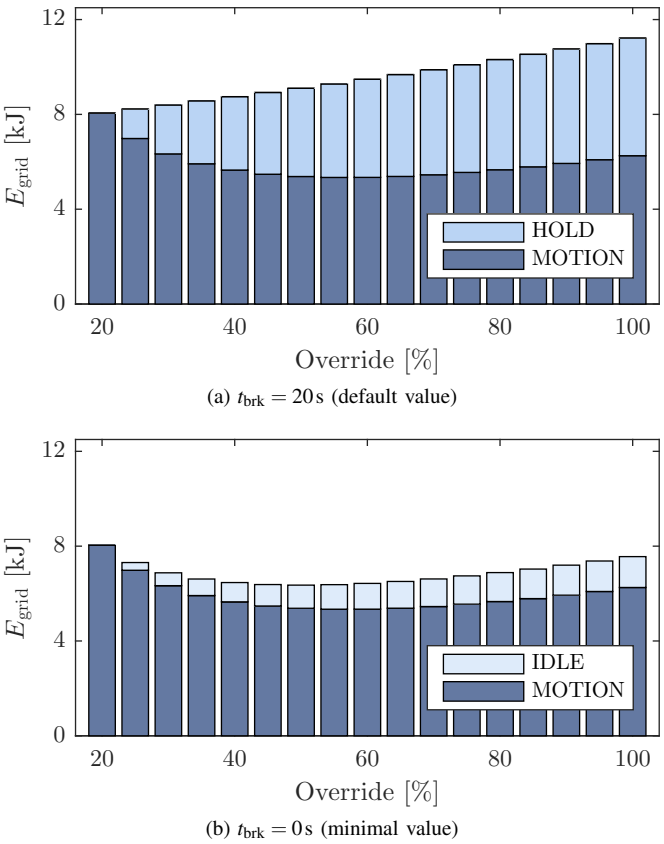

(a) $t_{\mathrm{brk}} = 20\,\mathrm{s}$ (default value)

(b) $t_{\mathrm{brk}} = 0\,\mathrm{s}$ (minimal value)

Fig. 8. Energy consumption over OR for an examplary task with different brake application times

50 % of all values. The ends of the antenna-like whiskers denote the range of approx. 99 % of all values. The red crosses represent outliers that occur from exceptional motions, e. g. single axis motions with a short distance. It can be seen that the shape of the graphic largely resembles the evaluation of a single motion as depicted in Fig. 8a. The graphic also depicts the expectable energy saving potential with regard to the OR (and, therefore, with regard to the travel time). Further evaluations show that the energy consumption always decreases with a reduction of the OR. The energy-optimal OR is the minimal value (here OR 20) in all regarded cases.

For the idealized brake application time $t_{\mathrm{brk}} = 0\,\mathrm{s}$, the results become less monotonous. The corresponding box plot is shown in Fig. 9b. It can be seen that an increase of travel time up to approx. 200 % (equals OR 50) still leads to energy savings in most cases. Since constant losses are higher during motion than in standstill, slower motions can feature even higher energy consumptions than the initial one at OR 100. The upper outliers are a result from motions with low mechanical power demands (e. g. wrist-only motions) where the brakes' share on the overall energy consumption is comparatively high. Energy-optimal ORs for this scenario can be found in Fig. 10a. A further evaluation reveals that the energy-optimal OR lies within the range of OR 40 to OR 60 for 90.2 % of the regarded motions. Further, an utilization of OR 50 leads to a reduction of energy consumption in 98.7 %

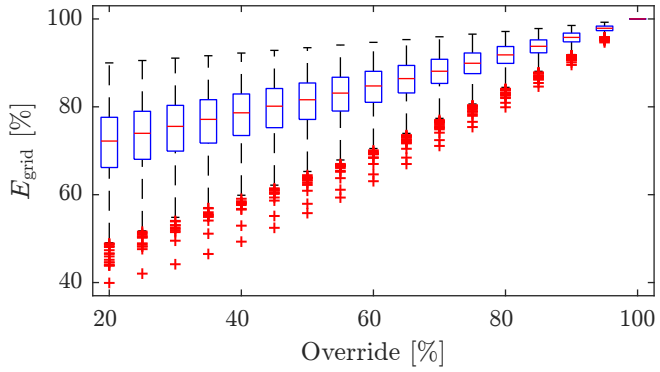

(a) $t_{\text{brk}} = 20\,\text{s}$ (default value)

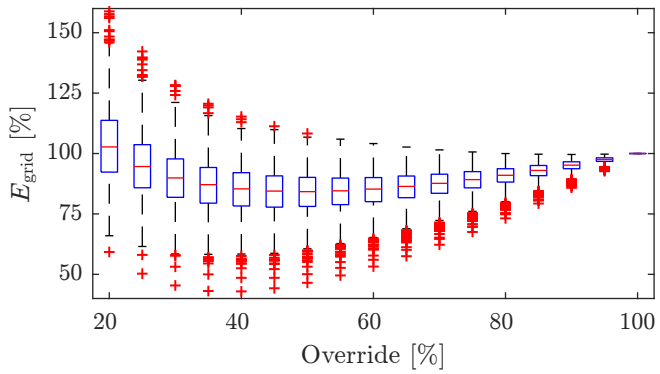

(b) $t_{\text{brk}} = 0\,\text{s}$ (minimal value)

Fig. 9. Energy consumption over OR for 1000 tasks with different brake application times

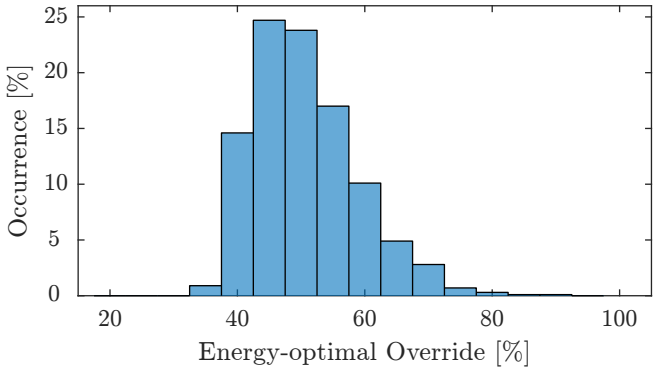

(a) Energy-optimal ORs with their respective occurrences with $t_{\text{brk}} = 0\,\text{s}$

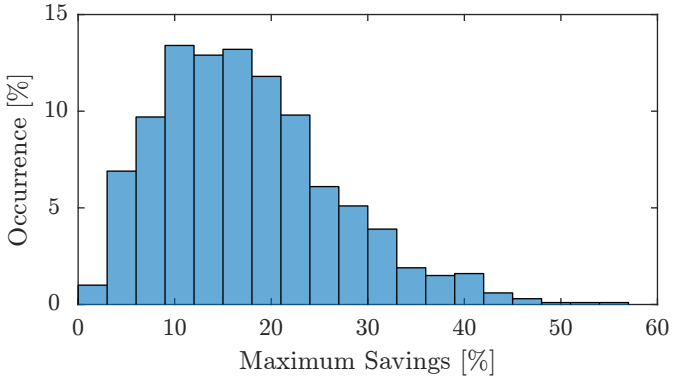

(b) Energy saving potential when applying energy-optimal OR with $t_{\text{brk}} = 0\,\text{s}$

Fig. 10. Detailed depiction of energy-optimal ORs and resulting energy saving potential at $t_{\text{brk}} = 0\,\text{s}$

of the cases. The resulting maximum savings at $t_{\text{brk}} = 20\,\text{s}$ can be read directly from the most left box in 9a, with the median being at 72 % (or 28 % savings). At $t_{\text{brk}} = 0\,\text{s}$, savings at optimal OR are depicted in Fig. 10b.

The evaluation results can be summarized as follows:

- The energy saving potential resulting from increase of travel time is highly dependent on the peripheral circumstances, such as constant consumer losses and/or brake control.
- For systems with high brake application times (current industrial standard), the slowest motion is the most efficient one in all regarded cases.
- An energy-efficient brake control system reduces the saving potential from the reduction of travel time. However, efficient brake control is always desirable and is only limited by allowed brake cycles.
- For most motions, an increase of travel time can be utilized to reduce energy consumption.

V. Conclusion and Future Work

This paper presented an approach to evaluate the relation between energy consumption and travel time. First, an energy modelling approach specifically designed for industrial robots has been introduced and validated at two different test rigs. In constrast to existing models, the presented one provides high accuracy with a significantly reduced set of additional parameters. The model was validated for two robots with differing sizes and payloads. In order to produce reliable results for a significantly larger set of motions than in existing publications, a method for automatic trajectory generation has been developed. Hence, the given results are mainly independent of the considered motion. General energy saving potentials were given and possible influences of other parameters (e. g. brake application time) were demonstrated.

Future work will focus on experimental validation and implementation on selected industrial production lines. Further, combination of the presented and other optimization approaches (such as optimizing geometrical path and/or robot base positioning) shall be evaluated.

Acknowledgment

The authors would like to thank the KUKA Roboter GmbH for granting us access to their laboratories to perform power measurements on a KUKA KR 210.

References

[1] *World Record: 248.000 Industrial Robots Revolutionising the Global Economy*, IFR press release, International Federation of Robotics Std., 06 2016. [Online]. Available: http://www.ifr.org/news/ifr-press-release/world-record-816/

[2] A. Albers, J. Ottnad, H. Weiler, and P. Haeussler, "Methods for lightweight design of mechanical components in humanoid robots," in *Proc. of the IEEE/RAS International Conference on Humanoid Robotics*, 2007, pp. 609–615.
[3] M. Akbaba, "Energy conservation by using energy efficient electric motors," *Applied Energy*, vol. 64, no. 1âĂŞ4, pp. 149–158, 1999.
[4] M. Brossog, M. Bornschlegl, J. Franke *et al.*, "Reducing the Energy Consumption of Industrial Robots in Manufacturing Systems," *The International Journal of Advanced Manufacturing Technology*, vol. 78, no. 5-8, pp. 1315–1328, 2015.
[5] D. Meike, M. Pellicciari, G. Berselli, A. Vergnano, and L. Ribickis, "Increasing the energy efficiency of multi-robot production lines in the automotive industry," in *Proc. of the IEEE International Conference on Automation Science and Engineering*, 2012, pp. 700–705.
[6] S. Riazi, K. Bengtsson, R. Bischoff, A. Aurnhammer, O. Wigström, and B. Lennartson, "Energy and peak-power optimization of existing time-optimal robot trajectories," in *Proc. of the IEEE International Conference on Automation Science and Engineering*, 2016, pp. 321–327.
[7] C. Hansen, J. Öltjen, D. Meike, and T. Ortmaier, "Enhanced Approach for Energy-Efficient Trajectory Generation of Industrial Robots," in *Proc. of the IEEE International Conference on Automation Science and Engineering*, 2012, pp. 1–7.
[8] K. Paes, W. Dewulf, K. Vander Elst, K. Kellens, and P. Slaets, "Energy Efficient Trajectories for an Industrial ABB Robot," *Procedia CIRP*, vol. 15, pp. 105–110, 2014.
[9] A. Vergnano, C. Thorstensson, B. Lennartson, P. Falkman, M. Pellicciari, F. Leali, and S. Biller, "Modeling and Optimization of Energy Consumption in Cooperative Multi-Robot Systems," *IEEE Transactions on Automation Science and Engineering*, vol. 9, no. 2, pp. 423–428, 2012.
[10] W. You, M. Kong, and L. Sun, "Optimal Motion Generation for Heavy Duty Industrial RobotsâĂŤControl Scheme and Algorithm," in *Proc. of the IEEE International Conference on Mechatronics*, 2011, pp. 528–533.
[11] D. Gleeson, S. Björkenstam, R. Bohlin, J. S. Carlson, and B. Lennartson, "Towards Energy Optimization Using Trajectory Smoothing and Automatic Code Generation for Robotic Assembly," *Procedia CIRP*, vol. 44, pp. 341–346, 2016.
[12] C. Hansen, J. Kotlarski, and T. Ortmaier, "Path Planning Approach for the Amplification of Electrical Energy Exchange in Multi Axis Robotic Systems," in *Proc. of the IEEE International Conference on Mechatronics and Automation*, 2013, pp. 44–50.
[13] M. Pellicciari, G. Berselli, F. Leali, and A. Vergnano, "A method for reducing the energy consumption of pick-and-place industrial robots," *Mechatronics*, vol. 23, no. 3, pp. 326–334, 2013.
[14] P. Hamon, M. Gautier, and P. Garrec, "Dynamic Identification of Robots With a Dry Friction Model Depending on Load and Velocity," in *Proc. of the IEEE/RSJ International Conference on Intelligent Robots and Systems*, 2010, pp. 6187–6193.
[15] C. T. Johnson and R. D. Lorenz, "Experimental identification of friction and its compensation in precise, position controlled mechanisms," *IEEE Transactions on Industry Applications*, vol. 28, no. 6, pp. 1392–1398, 1992.
[16] H. Abdellatif and B. Heimann, "On compensation of passive joint friction in robotic manipulators: Modeling, detection and identification," in *2006 IEEE Conference on Computer Aided Control System Design, 2006 IEEE International Conference on Control Applications, 2006 IEEE International Symposium on Intelligent Control*, Oct 2006, pp. 2510–2515.
[17] D. Meike, M. Pellicciari, and G. Berselli, "Energy Efficient Use of Multirobot Production Lines in the Automotive Industry: Detailed System Modeling and Optimization," *IEEE Transactions on Automation Science and Engineering*, vol. 11, no. 3, pp. 798–809, 2014.
[18] D. Meike and L. Ribickis, "Energy efficient use of robotics in the automobile industry," in *2011 15th International Conference on Advanced Robotics (ICAR)*, 2011, pp. 507–511.